REPORT DOCUMENTATION PAGE

Form Approved
OMB No. 0704-0188

1. REPORT DATE *(DD-MM-YYYY)*	**2. REPORT TYPE**	**3. DATES COVERED** *(From - To)*
18-01-2007	Journal Article	

4. TITLE AND SUBTITLE

Laser-induced Fluorescence Measurements of Velocity within a Hall Discharge

5a. CONTRACT NUMBER

5b. GRANT NUMBER

5c. PROGRAM ELEMENT NUMBER

6. AUTHOR(S)
W.A. Hargus, Jr. (AFRL/PRSS); M.A. Cappelli (Stanford University)

5d. PROJECT NUMBER
10110009

5e. TASK NUMBER

5f. WORK UNIT NUMBER

7. PERFORMING ORGANIZATION NAME(S) AND ADDRESS(ES)

Air Force Research Laboratory (AFMC)
AFRL/PRSS
1 Ara Drive
Edwards AFB CA 93524-7013

8. PERFORMING ORGANIZATION REPORT NUMBER

AFRL-PR-ED-JA-2007-033

9. SPONSORING / MONITORING AGENCY NAME(S) AND ADDRESS(ES)

Air Force Research Laboratory (AFMC)
AFRL/PRS
5 Pollux Drive
Edwards AFB CA 93524-70448

10. SPONSOR/MONITOR'S ACRONYM(S)

11. SPONSOR/MONITOR'S NUMBER(S)
AFRL-PR-ED-JA-2007-033

12. DISTRIBUTION / AVAILABILITY STATEMENT

Approved for public release; distribution unlimited (AFRL-ERS-PAS-2007-033)

13. SUPPLEMENTARY NOTES
Published in Applied Physics B, 72, 961-969 (2001).

14. ABSTRACT

The results of a study of laser-induced fluorescence velocimetry of neutral and singly ionized xenon in the plume and interior portions of the acceleration channel of a Hall thruster plasma discharge operating at powers ranging from 250 to 725 W are described. Axial ion and neutral velocity profiles for four discharge voltage conditions (100V, 160V, 200V, 250V) are measured as are radial ion velocity profiles in the near-field plume. Ion velocity measurements of axial velocity both inside and outside the thruster as well as radial velocity measurements outside the thruster are performed using laser-induced fluorescence with nonresonant signaldetection on the xenon ion 5d[4]7/2–6p[3]5/2 excitation transition while monitoring the signal from the 6s[2]3/2–6p[3]5/2 transition. Neutral axial velocity measurements are similarly performed in the interior of the Hall thruster using the 6s[3/2]02–6p[3/2]2 transition with resonance fluorescence collection. Optical access to the interior of the Hall thruster is provided by a 1-mm-wide axial slot in the insulator outer wall. While the majority of the ion velocity measurements used partially saturated fluorescence to improve the signal-to-noise ratio, one radial trace of the ion transition was taken in the linear fluorescence region and yields a xenon ion translational temperature between 400 and 800 K at a location 13 mm into the plume.

15. SUBJECT TERMS

16. SECURITY CLASSIFICATION OF:			**17. LIMITATION OF ABSTRACT**	**18. NUMBER OF PAGES**	**19a. NAME OF RESPONSIBLE PERSON**
					Dr. James Haas
a. REPORT	**b. ABSTRACT**	**c. THIS PAGE**	SAR	10	**19b. TELEPHONE NUMBER** *(include area code)*
Unclassified	**Unclassified**	**Unclassified**			N/A

Appl. Phys. B 72, 961–969 (2001) / Digital Object Identifier (DOI) 10.1007/s003400100589

Applied Physics B
Lasers
and Optics

Laser-induced fluorescence measurements of velocity within a Hall discharge

W.A. Hargus, Jr.*, M.A. Cappelli

Mechanical Engineering Department, Thermosciences Division, Stanford University, Stanford, CA 94305, USA

Received: 27 September 2000/Revised version: 2 March 2001/Published online: 9 May 2001 –

Abstract. The results of a study of laser-induced fluorescence velocimetry of neutral and singly ionized xenon in the plume and interior portions of the acceleration channel of a Hall thruster plasma discharge operating at powers ranging from 250 to 725 W are described. Axial ion and neutral velocity profiles for four discharge voltage conditions (100 V, 160 V, 200 V, 250 V) are measured as are radial ion velocity profiles in the near-field plume. Ion velocity measurements of axial velocity both inside and outside the thruster as well as radial velocity measurements outside the thruster are performed using laser-induced fluorescence with nonresonant signal detection on the xenon ion $5d[4]_{7/2}$–$6p[3]_{5/2}$ excitation transition while monitoring the signal from the $6s[2]_{3/2}$–$6p[3]_{5/2}$ transition. Neutral axial velocity measurements are similarly performed in the interior of the Hall thruster using the $6s[3/2]^0_2$–$6p[3/2]_2$ transition with resonance fluorescence collection. Optical access to the interior of the Hall thruster is provided by a 1-mm-wide axial slot in the insulator outer wall. While the majority of the ion velocity measurements used partially saturated fluorescence to improve the signal-to-noise ratio, one radial trace of the ion transition was taken in the linear fluorescence region and yields a xenon ion translational temperature between 400 and 800 K at a location 13 mm into the plume.

PACS: 52.70.Kz; 52.75.Di; 52.80.Vp

Due to their high specific impulse and high thrust efficiencies, Hall thrusters are now being considered for use on commercial, research, and military spacecraft. This technology provides economic advantages for a number of missions and its use can be translated into lower launch mass, longer time on station, or larger payloads [1]. In order to extend the performance and operating envelope of Hall thrusters, there is a need for increased understanding of the complex phenomena that control propellant ionization and acceleration within the discharge. In order to more fully understand the physics in these discharges, several laboratory-model Hall thrusters have been constructed at Stanford University. These thrusters serve as test articles for model development and advanced plasma diagnostics, including laser-induced fluorescence (LIF), probes of various types, and thrust measurements [2–5].

Laser-based techniques have been developed to nonintrusively probe neutral and ionized xenon [2, 5]. Such measurements in the plumes of Hall and other types of ion thrusters provide important information on the expansion of the plasma plume and its potential effect on satellite propulsion design and integration. Laser-based diagnostic measurements have been previously employed to examine plume plasma properties in other electric propulsion devices. For example, the hydrogen arcjet has been extensively studied using lasers to measure velocity, temperature, and electron number density [6]. However, few measurements (especially optical measurements) have been made within the interior discharge of these devices. The high spatial resolution of single-point LIF is essential in probing nonuniform plasma environments such as those inside Hall thrusters and other electric propulsion devices.

Ion velocity measurements of axial velocity, both inside and outside the thruster as well as radial velocity measurements outside the thruster, are performed using LIF with nonresonant signal detection exciting the xenon ion $5d[4]_{7/2}$–$6p[3]_{5/2}$ electronic transition while monitoring the signal from the $6s[2]_{3/2}$–$6p[3]_{5/2}$. Neutral axial velocity measurements are similarly performed in the interior of the Hall thruster using the $6s[3/2]^0_2$–$6p[3/2]_2$ transition with resonance fluorescence collection. The majority of the velocity measurements use partially saturated fluorescence to improve the signal-to-noise ratio.

1 Theory

1.1 Laser-induced fluorescence

Laser-induced flourescence is used to detect velocity-induced shifts in the spectral absortpion of xenon atoms and ions. The fluorescence is monitored as a continuous-wave laser is tuned in frequency over the transition of interest, of energy $h\nu_{12}$.

*Corresponding author.
Now located at Air Force Research Laboratory, Spacecraft Propulsion Branch, Edwards AFB, CA 93534, USA

Measurements can be made with high spatial resolution, determined by the intersection of the probe laser beam with the fluorescence optical collection volume.

In laser-induced fluorescence velocimetry, an atom or ion moving with a velocity component u relative to the direction of the incoming laser will absorb the light at a frequency shifted from that of stationary absorbers due to the Doppler effect. The magnitude of this frequency shift $\delta\nu_{12}$ is

$$\delta\nu_{12} = \nu_{12}\frac{u}{c}\,. \tag{1}$$

The measured fluorescence signal is given by [7–9]:

$$s_{\mathrm{f}} = \eta_{\mathrm{d}}\alpha_{\mathrm{c}} h\nu_{12} A_{21} N_2\,, \tag{2}$$

where η_{d} is the efficiency of the detection system, α_{c} accounts for geometric factors involving the collection system, and A_{21} is the Einstein coefficient for spontaneous emission of the relevant transition. For low laser intensities, rate equation analysis indicates that the upper level population N_2, and therefore the fluorescence signal, is linearly dependent on laser intensity at steady state, i.e.

$$N_2 \sim I_\nu B_{12}\phi_\nu\,, \tag{3}$$

where I_ν is the spectral irradiance at frequency ν, B_{12} is the Einstein stimulated absorption coefficient, and ϕ_ν is the transition's spectral line shape, which accounts for the variation of the absorption or laser excitation with frequency. The line shape is determined by the environment of the absorbing atoms, so an accurate measurement of the line shape function can lead to the determination of various plasma parameters. However, for velocity measurements, partially saturated fluorescence with a distorted line shape can still provide an adequate measure of the mean velocity. This was experimentally verified with several saturation studies which also examine the Doppler shift. The variation of the resultant velocities was found, in this study, to be less than the experimental uncertainty for the ions ($\pm$500 m/s), or for the neutrals ($\pm$60 m/s).

Several factors affect the line shape and give rise to broadening and/or a shift of the spectral line. In high-temperature plasmas, the most significant is Doppler broadening due to the absorber's random thermal motion, characterized by the molecular kinetic temperature, T_{kin}. When the absorbing species velocity distribution is Maxwellian in shape, the Doppler broadening results in a Gaussian line shape. Collisional interactions between the absorbers and other species in the plasma give rise to spectral line shapes that are often Lorentzian. This includes interactions with charged particles (Stark broadening) and uncharged particles (van der Waals broadening). If both Doppler broadening and collisional broadening are important and independent, the resulting line shape is a convolution of the Gaussian and Lorentzian line shape into a Voigt line shape [9].

The absorption line shape is an intrinsic property of the absorbers, whereas the fluorescence excitation line shape is the variation in the detected fluorescence signal with frequency as the laser is tuned across the absorption line feature. If the laser excitation significantly perturbs the populations of the coupled levels, it is said to be saturating the transition and the fluorescence signal is then a nonlinear function of laser intensity. In cases where the laser intensity is significantly below the saturation level and the laser linewidth is small compared to the measured linewidth, the fluorescence excitation line shape reflects the spectral absorption line shape as given by (2) and (3). When the laser intensity is sufficiently high to saturate the transition, the fluorescence excitation line shape is broader than the spectral line shape and the fluorescence intensity is less than it would be if it were linear with the laser intensity I_ν. The saturation intensity, defined as that intensity which produces a fluorescence signal half of what it would be if the fluorescence was linear with I_ν, depends inversely on the line strength of the particular transition. Stronger transitions have a smaller saturation intensity and thus a larger saturation effect for a given laser intensity.

1.2 Hyperfine structure

The nine isotopes of xenon, the propellant most commonly used in Hall plasma thrusters, each have a slight difference in their electron transition energies due to their differences in mass [10]. The odd mass isotopes are further spin split due to nuclear magnetic dipole and electric quadrapole moments. Nuclei which have an odd number of protons and/or an odd number of neutrons possess an intrinsic nuclear spin $Ih/2\pi$, where I is integral or half-integral depending on if the atomic mass is even or odd, respectively [11]. For nuclei with nonzero nuclear spin (angular momentum), the interaction of the nucleus with the bound electrons lead to the splitting of levels with angular momentum J into a number of components, each corresponding to a specific value of the total angular momentum $F = I + J$ [12]. As a result of this interaction, F is a conserved quantity while I and J individually are not. The interaction is weak, allowing the hyperfine splitting of each level to be taken independently of the other levels. The number of nuclear spin split hyperfine components is $2I+1$ if $J \geq 1$ and $2J+1$ if $J < 1$, with F taking on the values $F = J + I,\ J + I - 1,\ \ldots,\ |J - I|$ [12, 13] while satisfying the selection rules imposed on F, i.e. $\Delta F = 0, \pm 1$, unless $F = 0$, in which case $\Delta F \neq 0$.

With these selection rules on the quantum numbers for a particular electronic transition, and with knowledge of the hyperfine structure constants which characterize the magnetic dipole and electric quadrupole moments of the nucleus [11], the hyperfine energy shifts from the position of the energy for the unshifted level with angular momentum J can be easily calculated [13]. The relative intesities of transitions between these levels is derived assuming Russel–Saunders coupling [13], allowing the complete construction of the fluorescence lineshape. Of course, the intensities of the isotope shifted transitions are proportional to each isotope's relative abundance [11, 14, 15]. The relative intensities of the nuclear spin split hyperfine splitting are governed by two summation rules [12]. First, the sum of the intensities of all the lines of the hyperfine structure of a transition $J \rightarrow J'$(the prime refers to the upper level involved in the transition) originating from a component F of the level J is proportional to the statistical weight of this component, $2F+1$. Second, the sum of the intensities of all the lines of the hyperfine structure, the transition $J \rightarrow J'$ ending on the component F' of the level J' is proportional to the statistical weight of this component, $(2F'+1)$. With these two sum rules, a system of linear equations is solved for the relative intensities of the nuclear spin split components of each isotope.

1.3 Xenon spectroscopy

For the results reported here, we probed the 823.2 nm and 834.7 nm electronic transitions of neutral and singly ionized xenon, respectively. The isotopic and nuclear-spin effects contributing to the hyperfine structure of the $6s[3/2]^0_2$–$6p[3/2]_2$ neutral xenon transition at 823.2 nm produced 21 spectral lines, 15 of which are shown in the transition schematic in Fig. 1a (the other six are of the same transition shown for the even isotopes). Similarly, the $5d[4]_{7/2}$–$6p[3]_{5/2}$ xenon ion transition at 834.7 nm has a total of 19 isotopic and spin split components, 13 of which are shown in Fig. 1b (again, the other six are of the same transition shown for the even isotopes). The hyperfine splitting constants are only known for a limited set of energy levels [16–20]. While isotope shifts and all of the hyperfine splitting constants are available for the upper and lower levels of the neutral 823.2 nm transition, the 834.7 nm xenon ion transition only has data on the nuclear spin splitting constants of the upper state, and no information is available on the transition-dependent isotope shifts. For LIF measurements primarily aimed at determining velocities within the plasma flow, it is often convenient to probe more accessible transitions for which there is incomplete knowledge of the isotopic and nuclear spin splitting constants. Manzella has shown that the $5d[4]_{7/2}$–$6p[3]_{5/2}$ xenon ion transition at 834.7 nm may be used to make velocity measurements in a Hall thruster plume [21]. A convenient feature of this transition is the presence of a relatively strong line originating from the same upper state ($6s[2]_{3/2}$–$6p[3]_{5/2}$ transition at 541.9 nm) which allows for nonresonant fluorescence collection [22]. A nonresonant fluorescence scheme is preferred where there is the possibility of laser scattering from internal surfaces of the discharge.

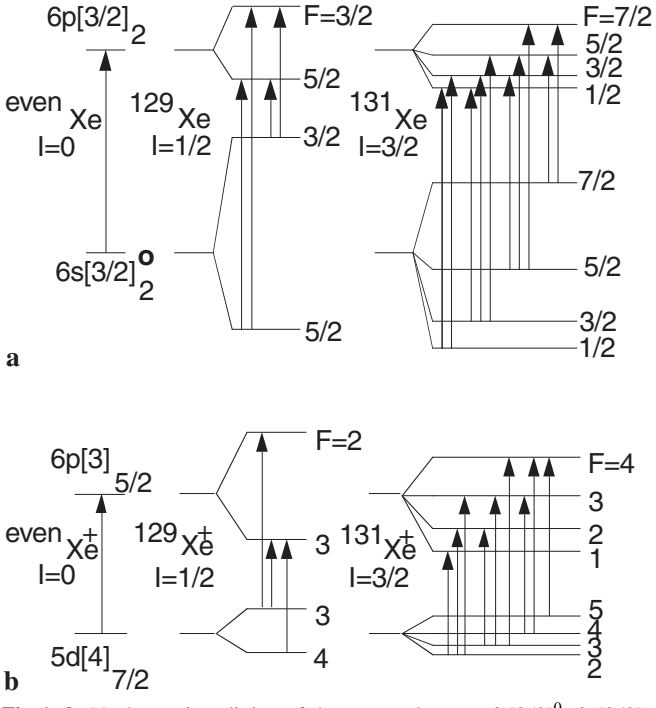

Fig. 1a,b. Nuclear spin splitting of the **a** neutral xenon $6s[3/2]^0_2$–$6p[3/2]_2$ and **b** singly ionized xenon $5d[4]_{7/2}$–$6p[3]_{5/2}$ transitions

2 Experiment

2.1 Test facility

The test facility consists of a non-magnetic cylindrical stainless-steel vacuum vessel 1 m in diameter and 1.5 m in length, pumped by two 50-cm diffusion pumps (backed by a 425 l/s mechanical pump) mounted at each end. Figure 2 shows a schematic of the facility. The base pressure with no flow is approximately 10^{-6} Torr as measured by an ionization gauge calibrated for nitrogen. Chamber pressures during discharge operation result in pressures of approximately 10^{-4} Torr (3×10^{-5} Torr on xenon, $\pm 50\%$). Gas flow to the Hall thruster anode and cathode is throttled by two Unit Instruments 1200 series mass flow controllers, factory-calibrated for xenon. The gas (propellant) used in this study was research grade (99.995%) xenon.

The thruster is mounted on a two-axis translation system having a vertical range of travel of 30 cm and axial (horizontal) range of 8 cm, each with a resolution of about 10 μm. Although the repeatability is considerably courser, it is still significantly less than the dimensions of the laser probe volume in the axial dimension. For internal LIF measurements, the thruster is mounted on a platform that provides optical access through a slot machined into the acceleration channel wall (described below). The view of the thruster mounting scheme is also shown in Fig. 2.

2.2 Hall thruster

The thruster used in this study has been described in detail extensively elsewhere [4]. It has four outer magnetic windings and a single inner winding generating the magnetic field, which is a maximum near the discharge exit plane. The insulator is constructed from two sections of cast alumina tubing 84 mm in length cemented to a machinable alumina back plate. The anode, which also serves as the gas distributer, is positioned at the back of the discharge channel constructed from the coaxial assembly of the alumina tubes. The channel has an outer diameter of 95 mm and a 12 mm width. A cross-sectional view of the assembled discharge thruster is shown in Fig. 3. Not shown in Fig. 3 is the external hollow cathode (ion Tech HCN-252), positioned with its orifice 20 mm beyond the

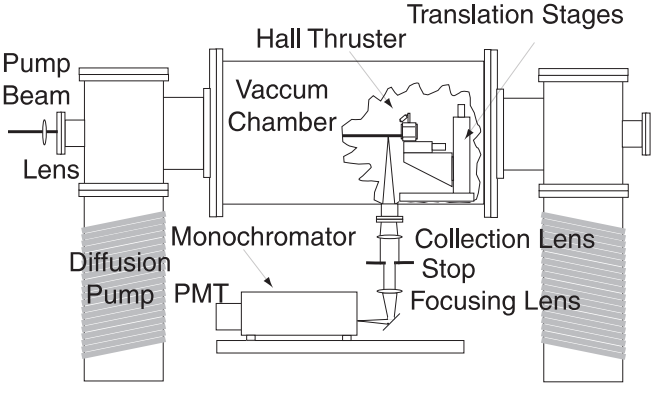

Fig. 2. Stanford high-vacuum facility, collection optics, and LIF probe beam access for axial velocimetry with a cutaway view showing mounted Hall thruster

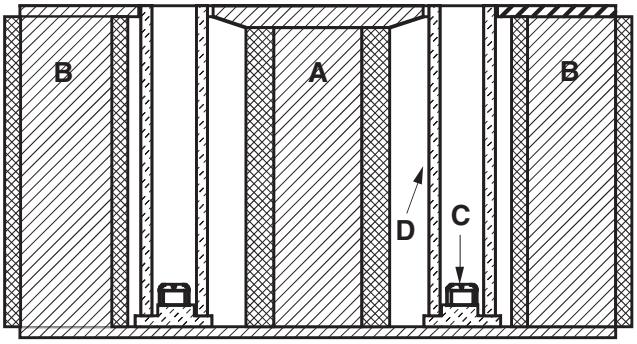

Fig. 3. Cross-section of the Stanford Hall thruster. A Central iron core. B Outer iron cores. C Anode and propellant distribution system. D Alumina insulator

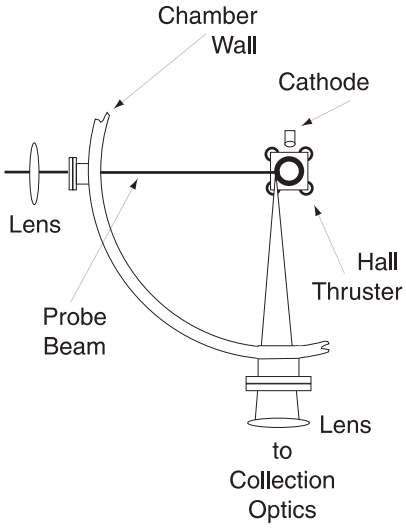

Fig. 4. LIF probe beam access for radial velocimetry

thruster exit plane, used to neutralize the ion beam and sustain the anode discharge.

For the LIF studies within the discharge chamber, a slot parallel to the axis 1 mm wide was machined into the outer insulator. The slot width was selected to be less than the local electron Larmor radius to minimize its influence on the discharge properties. The slot provides optical access to the interior of the Hall thruster, and operation with the slot did not differ significantly from the operation with the unslotted insulator (identical current–voltage characteristics). Despite the presence of the slot, optical access to the interior is still limited near the exit plane by the front plate of the magnetic circuit, precluding optical measurements very near the exit plane. The front iron plate is not cut since this would modify the local magnetic field.

2.3 Laser-induced fluorescence

The experimental apparatus used for the LIF measurements includes a tunable Coherent 899-21 single-frequency titanium sapphire laser, actively stabilized to provide linewidths on the order of 1 MHz with near zero frequency drift. The titanium sapphire laser is pumped by a Coherent Nd:YAG solid-state Verdi pump laser, which provides 5 W of single mode pump power at 532 nm. The tunable laser wavelength is monitored by a Burleigh Instruments WA-1000 scanning Michelson interferometer wavemeter with a resolution of 0.01 cm^{-1}.

The laser beam is chopped to allow for phase-sensitive detection and directed into the Hall thruster plume by a series of mirrors. For axial velocimetry measurements, the slightly divergent beam (1.7 mrad full angle) is focused to a sub-millimeter beam waist by a 50-mm-diameter 1.5-m-focal-length lens, as shown in Fig. 2. For radial velocimetry measurements, the beam enters through a side window and is focused by a 50-mm-diameter, 50-cm-focal length lens, as shown in Fig. 4. The collection optics for both radial and axial velocity measurements consist of a 75-mm-diameter 60-cm-focal-length collimating lens. The collected light is then focused on to the entrance slit of a 0.5-m Ebert–Fastie monochromator with a 50-mm-diameter 30-cm-focal-length lens. An optical field stop is placed between the two lenses to match the $F/\#$ of the optical train with that of the monochromator. The monochromator is used in the collection optical train as a narrow-band optical filter so that only light from the transition of interest is collected. With entrance and exit slits fully open (425 μm), the 600 groove/mm plane grating (blazed for 600 nm) within the monochromator allows the exit slit mounted Hamamatsu R928 photomultiplier tube (PMT) to sample a wavelength interval of approximately 1 nm. The orientation of the monochromator allows the slit aperture to define the length of the probe beam along which the fluorescence is collected. The sample volume for the axial data presented in this work is approximately 100 μm in diameter and 2 mm in length. Similarly, the sample volume of the radial data is approximately 100 μm in diameter and 1 mm in length. For neutral xenon LIF velocimetry measurements, a portion of the probe beam is split from the main beam, passed through a xenon glow discharge tube, and used as a stationary absorption reference. A silicon photodiode monitors the absorption signal. This use of the glow discharge tube is only possible for neutral xenon. The glow discharge does not support a sufficient population of excited state ions. However, the unshifted ion transition line center was confirmed to correspond to that taken from the literature by the observation of very slow moving ions near the anode, and by radial measurements near the acceleration channel center.

The probe laser beam is chopped, and the LIF signal is collected using a Stanford Research Systems SRS-850 digital lock-in amplifier. Concurrently, the absorption signal from the stationary reference is collected using an SRS-530 lock-in amplifier. Data from the absorption signal, laser power output, and the wavemeter are stored on the digital lock-in amplifier using three available analog inputs along with the LIF signal. Typical tests consist of a 12–20 GHz scan of the probe laser frequency over a 3-min period. The beam is chopped at a frequency of 1.5 kHz, and both lock-in amplifiers use 1-s time constants. Data is sampled at 8 Hz, producing four traces of approximately 2000 points for each velocity data point. Several unsaturated traces using lower laser intensities, 10-s time constants, and 10-min scans were also collected.

3 Results and analysis

The Hall thruster is operated at four conditions for the work reported here. At each condition, the peak magnetic field is

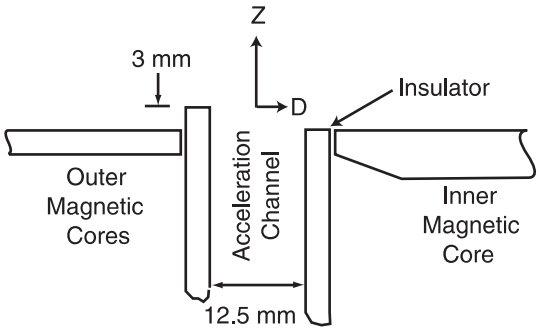

Fig. 5. Coordinate system for referencing locations of measurements

125 G, the mass flow to the anode is 2 mg/s, and the mass flow to the external hollow cathode is 0.3 mg/s. The test conditions correspond to discharge voltages of 100, 160, 200, and 250 V. The anode currents for these conditions are 2.1, 2.4, 2.6, and 2.9 A, respectively. The total power consumed by the cathode and magnet circuit is approximately 30 W. It should be noted that the power dissipated in the ballast resistors on the anode and cathode keeper lines ($\sim$ 10 W) is not included in these calculations.

All spatially resolved measurements are referenced to a two-coordinate system shown in Fig. 5. The position in the radial coordinate is referenced to the radial location corresponding to the midpoint of the acceleration channel using the variable D, defined as positive toward the thruster centerline. The axial coordinate is given by Z which is the distance from the thruster exit plane and is defined as positive along the thrust vector.

3.1 Saturation study

The $5d[4]_{7/2}$–$6p[3]_{5/2}$ xenon ion transition at 834.7 nm was probed to extract local velocity data from the Doppler shift of the measured fluorescence. Figure 6 shows the saturation curve of the transition at a location 13 mm from the exit plane at the center of the acceleration channel. Here, the laser beam is propagating normal to the thrust vector and the measurement is of the radial velocity component. A typical saturated trace (laser power of 20 mW) used to determine the velocity in the probed volume is compared to an unsaturated trace (laser power of 0.2 mW) from the same location in Fig. 7. Both traces are normalized in the figure to unity peak signal.

Velocity measurements of the saturation curve data making up Fig. 6 are shown in Fig. 8. The mean velocity for these data points yields a value of -62 m/s with a standard deviation of 65 m/s and a range of 127 m/s. The absolute accuracy of the measurements is limited by the specified uncertainty of the wavemeter reading, which is ± 500 m/s at this wavelength. The important conclusion that may be drawn from this data is that the $5d[4]_{7/2}$–$6p[3]_{5/2}$ xenon ion transition of xenon provides useful LIF velocimetry data even when partially saturated. This allows the collection of partially saturated fluorescence signals, maximizing the signal-to-noise ratio and/or allowing for faster scans while still being able to extract velocity data from the fluorescence signal. These measurements also serve as a confirmation of an improved accuracy of the unshifted wavelength since a finite radial velocity is not expected at this location. Similar results were also obtained in a neutral xenon LIF saturation study.

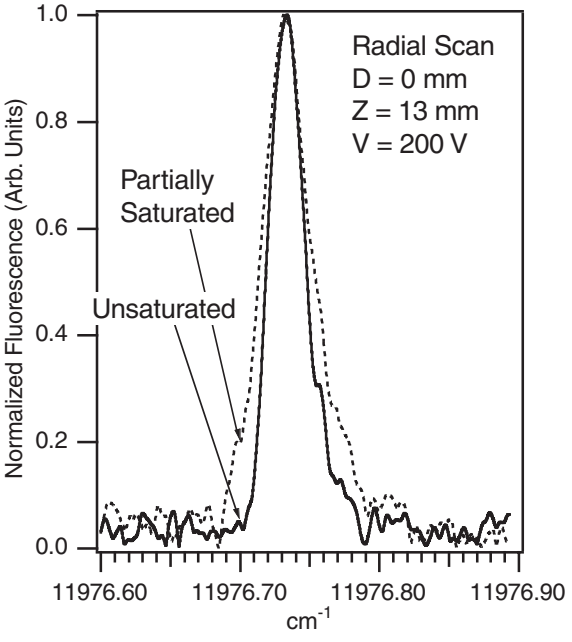

Fig. 7. Saturated (20 mW) and unsaturated (0.2 mW) radial xenon ion LIF traces for a discharge voltage of 200 V at $Z = 13$ mm, $D = 0$ mm

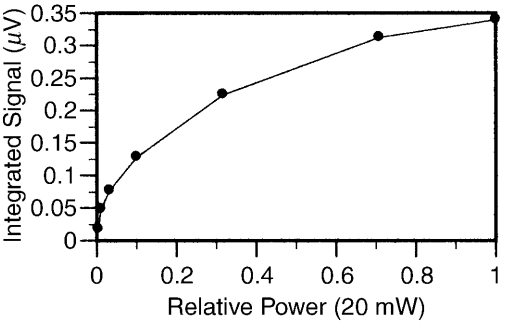

Fig. 6. Saturation curve of radial xenon ion measurements for an anode discharge voltage of 200 V at $Z = 13$ mm, $D = 0$ mm. Note the uncertainty of these measurements is primarily due to the uncertainty of the optical densities of the neutral density filters used for this measurement ($\pm 5\%$)

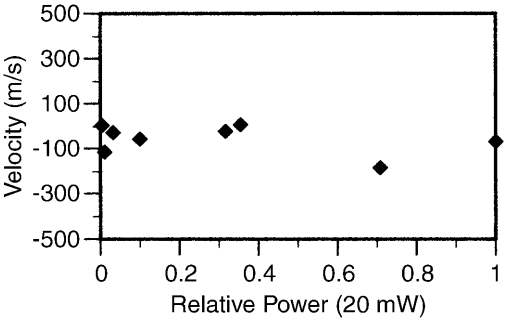

Fig. 8. Invariance of the measured radial xenon ion velocity in the saturation study shown in Fig. 7. Note that the uncertainty of the velocity measurements is approximately ± 500 m/s

3.2 Xenon ion LIF velocimetry

The axial LIF velocimetry measurements consist of two data sets for each operating condition. The first data set includes ion velocity measurements taken externally extending from the exit plane to approximately $Z = 35$ mm. The second data set contains internal axial velocity measurements taken from the exit plane to approximately $Z = -75$ mm. These ranges are imposed by the limited travel of the translation stage that provides axial motion to the Hall thruster. Axial velocimetry measurements were taken every 2.5 mm with a sample probe volume of 100 μm in diameter and 2 mm long. For several of the test conditions examined, profiles of the axial velocity across the coordinate D were also examined. Measurements of near-plume radial ion velocities were also performed. These measurements are limited to the plume due to the limited optical access to the interior of the Hall thruster.

The complete axial velocity profiles for the four cases examined are shown in Fig. 9. The error bars correspond to the ±500 m/s uncertainty associated with the determination of the magnitude of the Doppler shift relative to the unshifted line center. The axial velocity profiles exhibit the expected behavior. The velocity is near zero near the anode ($Z = -78$ mm), and begins to rise near $Z = -10$ mm at the edge of the acceleration zone. The ions are rapidly accelerated in the region of the exit plane and reach their full velocity in the neighborhood of $Z = 20$ mm. This latter position corresponds to the location of the hollow cathode neutralizer relative to the body of the thruster and is sometimes referred to as the cathode plane in the literature [21].

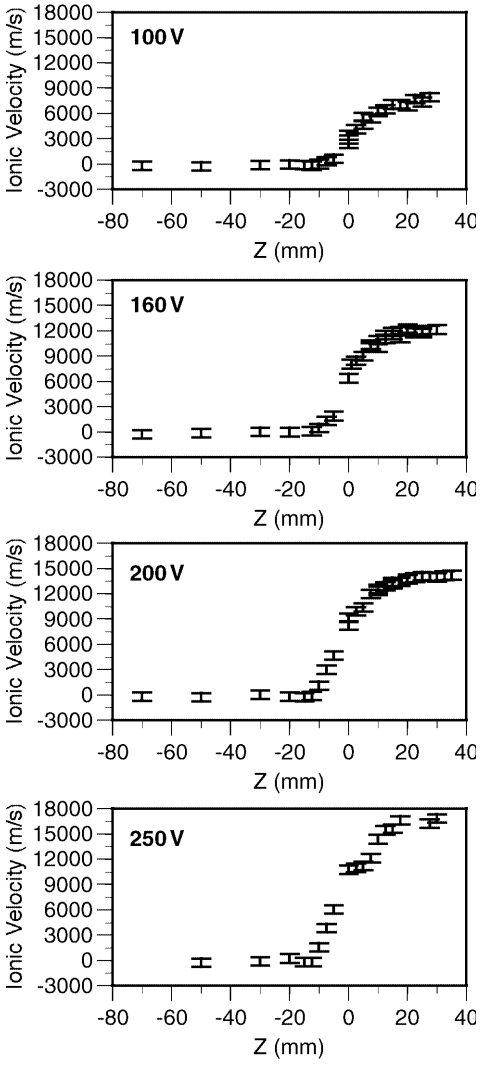

Fig. 9. Axial internal and external xenon ion velocity measurements at $D = 0$ mm for discharge voltages of 100 V, 160 V, 200 V, and 250 V

The length of the acceleration region in all cases is invariant at 30 mm. Therefore, increases in the anode potential result in a concomitant increase of the axial electric field component within the thruster acceleration channel. The initial acceleration is seen to begin at 10 mm within the thruster where the magnetic field has a value of approximately 85% of the centerline maximum. The propellant acceleration is completed 20 mm beyond the exit plane when the magnetic field has a value of approximately 25% of the centerline maximum.

Significant acceleration of the ionized propellant occurs outside the Hall thruster. This is consistent with the results first identified in a Hall discharge with a much shorter acceleration channel [2]. It is noteworthy that the velocity increment imparted to the propellant outside the Hall thruster is essentially constant, invariant to discharge voltage, with an average value of 5000 m/s. Only for the 100 V case does the majority of the acceleration occur outside the thruster. Higher discharge voltages appear to have a constant percentage of the acceleration occurring externally. It is also equally interesting to cast this result in terms of the kinetic energy of the propellant. In the case of the 100-V discharge operation, approximately 90% of the energy is deposited into the propellant between the exit and cathode planes. For the 250 V case, the fraction of energy deposition beyond the exit plane is nearer to 60%. It appears then that the majority of the energy deposition into the Hall thruster propellant occurs outside the thruster. However, since the thrust is equivalent to the momentum flux, the majority (65%) of the thrust is still generated within the thruster in all cases above 100 V. It is further noteworthy that in all the cases approximately 60 eV is unaccounted. This value is constant to within the uncertainties of the velocity measurement and implies that the mechanism responsible for this loss is invariant with the applied anode potential. This energy loss may be a product of the anode and cathode potential falls, or other mechanisms common to these discharges (e.g. distribution of the ion production, or resistive losses in regions of low ionization fractions). It is noted that these measurements are limited to axial velocities and do not account for losses due to plume divergence.

Several radial profiles of the axial ion velocity in Fig. 10 illustrate the radial variation of the measured axial velocities for a discharge voltage of 160 V at two locations in the plume and one within the thruster for a discharge voltage of 200 V. The width of the acceleration channel is 12 mm (-6 mm $< D < 6$ mm). The axial velocity profile is nearly flat which strongly implies lines of constant potential in the radial direction. The slightly concave distribution inside the channel (200-V case) is consistent with the expected equipotential surfaces associated with the radial magnetic field.

Radial velocity measurements were also performed in the plume. Combined with the above axial velocity measurements and the observation that the axial velocity appears to be independent of D, vector plots of the near plume may be constructed. Figure 11 shows a vector plot constructed for

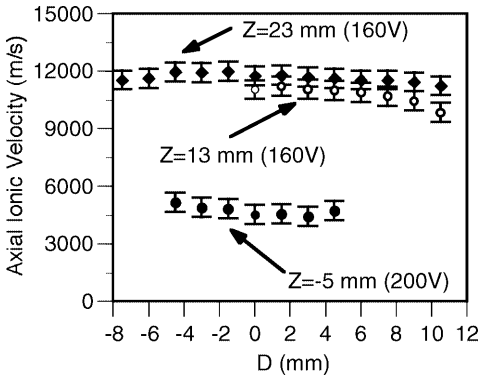

Fig. 10. Profiles of axial xenon ion velocity measurements for several discharge voltages and axial locations

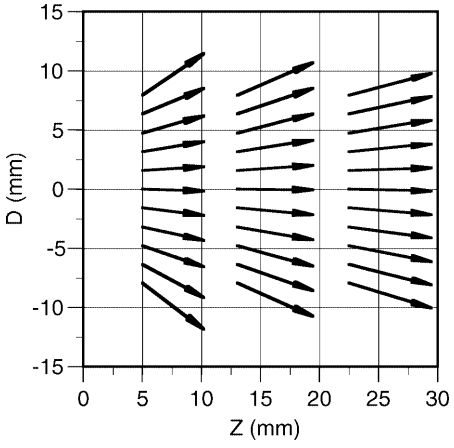

Fig. 11. External xenon ion velocity field calculated from radial and axial velocity measurements for a 200-V discharge voltage

a 200-V discharge voltage. In this case, radial velocities vary linearly with D with near zero velocity at $D = 0$ mm and peak at values above 6000 m/s as close as $Z = 13$ mm and $D = 8$ mm. A prominent feature of a Hall thruster plume is the luminous central cone originating at the thruster axis adjacent to the center pole piece. Although the propellant stream exits the thruster in an annulus, an intense, optically emitting conical feature extends a significant distance into the vacuum chamber (10–30 cm for our background pressures) and is especially evident at higher discharge voltages. The inward focus of the divergent propellant flow is likely a contributing mechanism in the formation of this intriguing feature which is not precisely understood.

3.3 Ion line shape analysis

The hyperfine splitting constants for the xenon ion $5d[4]_{7/2}$–$6p[3]_{5/2}$ transition at 834.7 nm are only known for the upper $6p[3]_{5/2}$ state. The isotope shifts for this transition are also unknown. While this does not greatly impact the accuracy to which velocities may be determined, it does impact the ability to use this transition for accurate measurements of the ion velocity distribution, or temperature. We point out here that the notion of a temperature for the ions in this flow is highly tenuous, as the ions may be treated kinetically, do not suffer many collisions, and are born (created) at distributed axial locations within the discharge. Furthermore, a time-averaged broadening of the fluorescence excitation spectra can arise due to oscillations in the zone of ionization. King has shown by mass and resolved energy analysis that the axial velocity of the ions has an energy distribution of approximately 10 eV (in the far field) due in part to the plasma oscillations within the Hall thruster [23]. The issue of the distribution of ion velocities due to the axial location where they were born is minimized by examining the fluorescence spectra in the radial direction. The spectra is taken from the position with the minimum measured velocity, approximately 100 m/s (±500 m/s) at a location of $D = 0$ mm and $Z = 13$ mm. In order for a temperature to be extracted from the measured lineshape, the ion population is assumed to be Maxwellian, or at least frozen in a close facsimile.

An estimate of the ion kinetic temperature with uncertainties of 40%–70% is possible. A radial excitation unsaturated fluorescence trace is shown in Fig. 12 and compared to a line shape model developed by Cedolin [24]. The model uses the $5d[3]_{7/2}$ lower level hyperfine spin splitting and isotopic shift data from the 605.1-nm transition and the measured splitting data for the $6p[3]_{5/2}$ upper level. Lorentzian broadening is neglected and only Doppler broadening is considered. The best fit of this model predicts a kinetic temperature of approximately 450 K. The model does not completely predict the outlying features, but this is expected since the spin splitting constants for the $5d[3]_{7/2}$ state are used for the lower level rather than those for the $5d[4]_{7/2}$ state probed here. If hyperfine splitting is ignored and only the isotope shifts corresponding to the values for the 605.1-nm transition are used, the model predicts a kinetic temperature of approximately 800 K. Neglecting all hyperfine splitting mechanisms, including isotopic and nuclear spin splitting, an upper bound on the temperature of 1700 K is determined from the fluorescence Doppler half-width. The uncertainty of this measurement is in large part due to the uncertainties of the spectral data as well as due to the noise in the fluorescence signal. A similar measurement in the plume of a SPT-100 by Manzella yielded a kinetic temperature of approximately 800 K [21]. It should be noted that Manzella used an incorrect value of J for the lower state which was first misidentified by Humphreys [25]

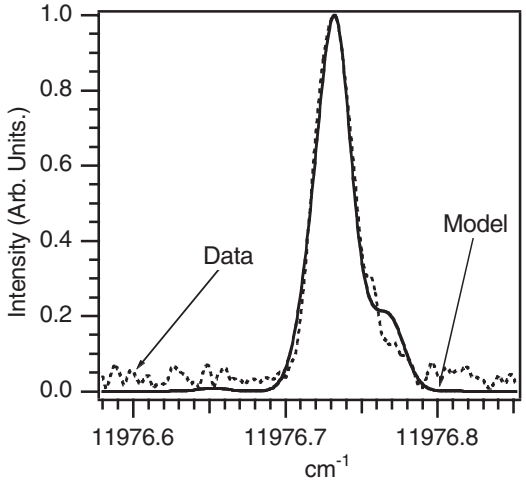

Fig. 12. Model fit to unsaturated radial xenon ion laser-induced fluorescence trace at a discharge voltage of 200 V, at a location of $D = 0$ mm and $Z = 13$ mm

and propagated by Moore [26] before finally being corrected by Hansen and Persson [22].

3.4 Neutral LIF velocimetry

Figure 13 shows the results of axial neutral xenon velocity measurements within the acceleration channel. The four cases examined show very similar behavior. The initial velocity near the anode is very low. The neutral velocity slowly rises until a position of approximately 20 mm within the thruster. At this point, where the ion acceleration is also seen to begin, the neutrals are accelerated at a higher rate until near the exit plane where the acceleration appears to slow and even possibly reverse when the thruster is operated at higher voltages. The decrease in neutral xenon velocity is likely due to thruster ingestion of background xenon. Since the effect appears to grow with increased discharge voltage, it is possible that a portion of the propellant flow reflected from nearby vacuum facility walls (now entirely consisting of neutrals) is ingested by the thruster.

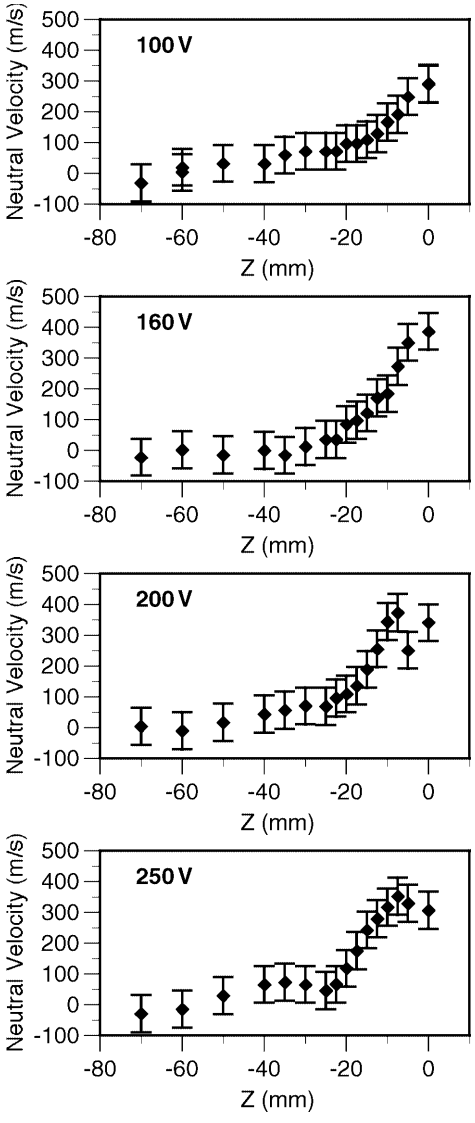

Fig. 13. Axial neutral velocity measurements at $D = 0$ mm for discharge voltages of 100 V, 160 V, 200 V, and 250 V

Flow from the cathode may be eliminated as the source of the apparent deceleration of the neutrals for a variety of reasons. First, the flow from the cathode, although 15% of the anode flow, is exiting from a 2-mm orifice approximately 12 cm above the sample volume. Flow from the cathode should be sufficiently diffuse and not affect the neutral velocity measurements in the sample volume. Second, the cathode is 2 cm downstream of the exit plane and angled 30° from the front plate pointed along the thrust axis. It is difficult to envision the cathode affecting the neutral velocity measurements within the acceleration channel. It is therefore almost certain that random neutral flux from the chamber background is responsible for the apparent drop in neutral velocity seen near the exit plane in Fig. 13.

Due to the highly nonequilibrium nature of the Hall thruster, it is important to understand the apparent acceleration of the neutrals beginning 40 mm upstream of the exit plane. The plasma within the Hall thruster is required to be of low collisionality by the constraint that the magnetic field limits the electron flux to the anode. The disparate velocities of the ions and neutrals strongly suggest that the neutral and ion populations are not coupled. As such, the apparent acceleration of the neutrals may actually be an artifact of the time of flight of the neutrals through the volumetric zone of ionization. Slower neutrals, or neutrals that travel a longer effective path length due to collisions with the walls of the acceleration channel, have a greater probability of being ionized than do neutrals in the high-energy portion of the velocity distribution. Therefore, neutrals from the high-energy range of the velocity distribution are more likely to reach the upstream portion of the acceleration channel. In this case, there is no actual acceleration of the neutrals, but rather a depletion of the slower moving neutrals by ionization.

The depletion of the slower neutral velocity classes accounting for the apparent acceleration of the neutrals as seen in Fig. 13 may be qualitatively explained by considering the one-dimensional Boltzmann equation [27].

$$u\frac{\partial}{\partial z}[n f(u)] = -[n f(u)] n_e S_i \,. \tag{4}$$

Where n is the neutral number density, u is the neutral velocity class, z is the spatial coordinate, $f(u)$ is the velocity distribution function, n_e is the local plasma electron number density, and S_i is the ionization rate coefficient. The generalized one-dimensional Boltzmann equation is simplified here by assuming the process is steady with no external forces and that the sole depletion mechanism for the neutral velocity classes is electron collisional ionization. Implicit in these assumptions is that the ions and neutrals do not significantly interact.

Equation (4) may be easily integrated with respect to $n f(u)$ to produce an analytic solution if the ionization rate coefficient S_i and the electron number density n_e are assumed to be constant. In this case, the population of the u velocity class $n f(u)$ exponentially decays with the spatial variable z moderated by the value of u

$$n f(u) \sim e^{-z/u} \,. \tag{5}$$

The qualitative conclusion drawn from this straightforward analysis of the one-dimensional Boltzmann equation is that the neutral density in a model plasma is depleted along

the Z-axis due to neutral–electron collisional ionization. This relative depletion depends on the velocity class. Neutrals in the lower velocity classes have a greater probability of being ionized when passing through the zone of ionization than neutrals of higher velocity classes. Therefore, the apparent acceleration of the neutrals in Fig. 13 is most likely the result of the depletion of the slower moving neutrals rather than an acceleration process.

4 Conclusions

Measurements of xenon ion and neutral velocities were performed in the plume and into the interior of the thruster through a 1-mm-wide slot in the outer insulator wall. From these measurements, information on propellant energy deposition, electric field strength, and flow divergence were extracted. Xenon ion velocity measurements of axial velocity both inside and outside the thruster as well as radial velocity measurements outside the thruster were performed using LIF with nonresonant signal detection using the xenon ion $5d[4]_{7/2}$–$6p[3]_{5/2}$ electronic transition while monitoring signal from the $6s[2]_{3/2}$–$6p[3]_{5/2}$ transition. Neutral velocity measurements were similarly performed in the interior of the Hall thruster using the $6s[3/2]^0_2$–$6p[3/2]_2$ transition with resonance fluorescence collection. Most velocity measurements used partially saturated fluorescence to improve the signal-to-noise ratio. One radial trace of the xenon ion transition was taken in the linear fluorescence region and yielded a plume ionic translational temperature between 400 and 800 K. However, since the hyperfine structure constants are not known for the $5d[4]_{7/2}$ level, the constants for the $5d[3]_{7/2}$ level were used instead. This result should therefore be viewed with caution. An upper limit on the kinetic temperature using only the full-width at half-maximum assuming no hyperfine splitting yields a temperature of 1700 K. From the neutral velocity measurements, the neutrals appear to be accelerated within the thruster. Conclusions drawn from analysis of the one-dimensional Boltzmann equation imply that neutrals are depleted along the Z-axis due to neutral-electron collisional ionization, and the relative depletion depends on the velocity class of the neutral atom. This preferentially depletes the lower velocity classes producing the apparent acceleration of the neutrals.

Acknowledgements. This work is supported by the Air Force Office of Scientific Research. W.A. Hargus, Jr. was supported under the Air Force Palace Knight Program.

References

1. S.W. Janson: AIAA 29th Joint Propulsion Conference 93-2220 (1993)
2. R.J. Cedolin, W.A. Hargus, Jr., P.V. Storm, R.K. Hanson, M.A. Cappelli: J. Phys. B **65** 459 (1997)
3. W.A. Hargus, Jr., N.B. Meezan, M.A. Cappelli: AIAA 33rd Joint Propulsion Conference 97-305 (1997)
4. W.A. Hargus, Jr., R.J. Cedolin, N.B. Meezan, M.A. Cappelli: AIAA 33rd Joint Propulsion Conference 97-3081 (1997)
5. W.A. Hargus, Jr., M.A. Cappelli: Propulsion and Power, submitted
6. P.V. Storm: *Thermosciences Division Report No. TSD-102: Optical Investigations of Plasma Properties in the Interior of Arcjet Thrusters* (Mech. Eng. Dept., Stanford University 1997)
7. R.P. Lucht: In *Laser Spectroscopy and its Applications* ed. by L.J. Radziemski, R.W. Solarz, J.A. Paisner (Marcel Dekker, New York 1987) pp. 623
8. A.C. Eckbreth: *Laser Diagnostics for Combustion Temperature and Species* (Overseas Publishers Association, Amsterdam 1996)
9. W. Demtröder: *Laser Spectroscopy: Basic Concepts and Instrumentation* (Springer-Verlag, Berlin 1996)
10. G. Herzberg: *Atomic Spectra and Atomic Structure* (Dover Publications, New York 1944)
11. R.D. Cowan: *The Theory of Atomic Structure and Spectra* (University of California Press, Berkley 1981)
12. I.I. Sobelman: *Atomic Spectra and Radiative Transitions* (Springer-Verlag, Berlin 1992)
13. H.E. White: *Introduction to Atomic Spectra* (McGraw-Hill Book Co., New York 1934)
14. D.R. Lidde (Ed.): *Handbook of Chemistry and Physics: 74th edn.* (CRC Press, Boca Raton 1993)
15. D.A. Jackson, M.C. Coulombe: Proc. R. Soc. Lond. A. **338**, 277 (1974)
16. G. Borghs, P. De Bisschop, R.E. Silerans, M. Van Hove, J.M. Van den Cruyce: At. Nucl. **299**, 11 (1981)
17. C.R. Bingham, M.L. Gaillard, D.J. Pegg, H.K. Carter, R.L. Mlekodaj, J.D. Cole, P.M. Grffin: Nucl. Instrum. Methods **202**, 147 (1982)
18. H. Geisen, T. Krumpelmann, D. Neuschafer, C. Ottinger: Phys. Lett. A **130**, 299 (1988)
19. W. Fischer, H. Huhnermann, G. Kromer, H.J. Schafer: Z. Phys. **270**, 113 (1974)
20. L. Bronstrom, A. Kastberg, J. Lidberg, S. Mannervik: Phys. Rev. A **53**, 109 (1996)
21. D.H. Manzella: AIAA 30th Joint Propulsion Conference 94-3141 (1994)
22. J.E. Hansen, W. Persson: Phys. Scr. **36**, 602 (1987)
23. L.B. King: *Transport-Property and Mass Spectral Measurements in the Plasma Exhaust Plume of a Hall-Effect Space Propulsion System* Ph.D. Dissertation, Aerospace Engineering, University of Michigan (1998)
24. R.J. Cedolin: *Thermosciences Division Report No. TSD-105: Laser-Induced Fluorescence Diagnostics of Xenon Plasmas*, Mech. Eng. Dept., Stanford University (1997)
25. C.J. Humpreys: J. Res. Nat. Bur. Stand. **22** 19 (1939)
26. C.E. Moore: *Atomic Energy Levels: Vol. III* (National Bureau of Standards, Washington 1958) pp. 113–123
27. W.G. Vincenti, C.H. Kruger, Jr.: *Introduction of Physical Gas Dynamics* (Krieger, Florida 1986)